NANO LETTERS

Letter

pubs.acs.org/NanoLett

Graded Recombination Layers for Multijunction Photovoltaics

Ghada I. Koleilat,[†] Xihua Wang,[†] and Edward H. Sargent*

Department of Electrical and Computer Engineering, University of Toronto, 10 King's College Road, Toronto, Ontario M5S 3G4, Canada

Supporting Information

ABSTRACT: Multijunction devices consist of a stack of semiconductor junctions having bandgaps tuned across a broad spectrum. In solar cells this concept is used to increase the efficiency of photovoltaic harvesting, while light emitters and detectors use it to achieve multicolor and spectrally tunable behavior. In series-connected current-matched multijunction devices, the recombination layers must allow the hole current from one cell to recombine, with high efficiency and low voltage loss, with the electron current from the next cell. We recently reported a tandem solar cell in which the recombination layer was implemented using a progression of n-type oxides whose doping densities and work functions serve to connect, with negligible resistive loss at solar current densities, the constituent cells. Here we present the generalized conditions for design of efficient graded recombination layer solar devices. We report the number of interlayers and the requirements on work function and doping of each interlayer, to bridge an work function difference as high as 1.6 eV. We also find solutions that minimize the doping required of the interlayers in order to minimize optical absorption due to free carriers in the graded recombination layer (GRL). We demonstrate a family of new GRL designs experimentally and highlight the benefits of the progression of dopings and work functions in the interlayers.

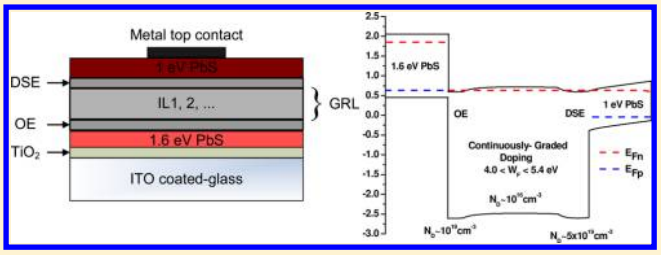

KEYWORDS: *Multijunction photovoltaics, tandem solar cell, graded recombination layer, thermionic and tunneling transport, transparent conductive oxides*

Multijunction solar cells raise the asymptote on solar-to-electric power conversion efficiency compared with single-junction solar cells.[1,2] Their constituent junctions can efficiently extract power from different portions of the broad solar spectrum: frontside wider-bandgap materials harvest high-energy photons, while abundant lower-energy photons are collected using the smaller-bandgap materials at the back of the stacked cell.[3]

Efficient transparent intermediate layers sandwiched between the junctions are essential to a current-matched multijunction solar cell.[4] They allow the photogenerated electrons and holes from adjacent junctions to meet and recombine efficiently with minimal optical and electrical loss. In traditional epitaxial compound semiconductor multijunction solar cells,[5] tunnel junctions are employed for this purpose. Degenerately doped p- and n-type materials produce an extremely thin (2−5 nm) junction in which the valence band on the p-side is energetically aligned with the n-side, and the depletion region is sufficiently thin that carriers can tunnel from one side to the other.[6,7] Since low-temperature-processed degenerately doped metal oxides represent a challenge in materials processing, solution-processed organic and inorganic cells require innovative solutions. In organic photovoltaics, multijunction solar cells employ recombination layers: electrons and holes recombine in metal nanoparticles inserted between the electron-transport and hole-transport layers.[8,9]

We recently reported a tandem solar cell employing a new recombination layer design tailored to be compatible with room temperature processing.[3] The device employed colloidal quantum dots that were tuned, through the quantum size effect, to provide the optical bandgaps needed in a tandem solar cell (Figure 1a). In the graded recombination layer (GRL) approach, a progression of readily available n-type transparent conductive oxides connects the front cell to the back cell.

The concept underlying the GRL is as follows: If a deep work function ohmic electrode (OE) to the front cell[10−12] were directly connected to a shallow work function electron acceptor in the back cell (Figure 1b,c),[13] a large energetic barrier would block the flow of electrons. This would prevent efficient recombination of these electrons with the holes generated in the front cell. This large energetic barrier for electrons could be reduced by building a continuously graded recombination layer that would connect the junctions and present no barrier to the flow of charge carriers (Figure 1d). Unfortunately, such a material—one that would continuously span the entire 1 eV work function separation of interest—is not readily available.

A more realistic strategy would employ a discrete set of intervening layers (IL1, 2, ...), each having an appropriate doping level, work function, and conductivity. This would enable electrons to flow across the recombination layer with an acceptable resistance in a photovoltaic device context (Figure 1e). For ease of experimental implementation, the approach would rely on transparent conductive n-type oxides having doping levels in the range of 10^{16}−10^{21} cm^{-3} work functions in the

Received: March 5, 2012
Revised: April 22, 2012
Published: May 3, 2012

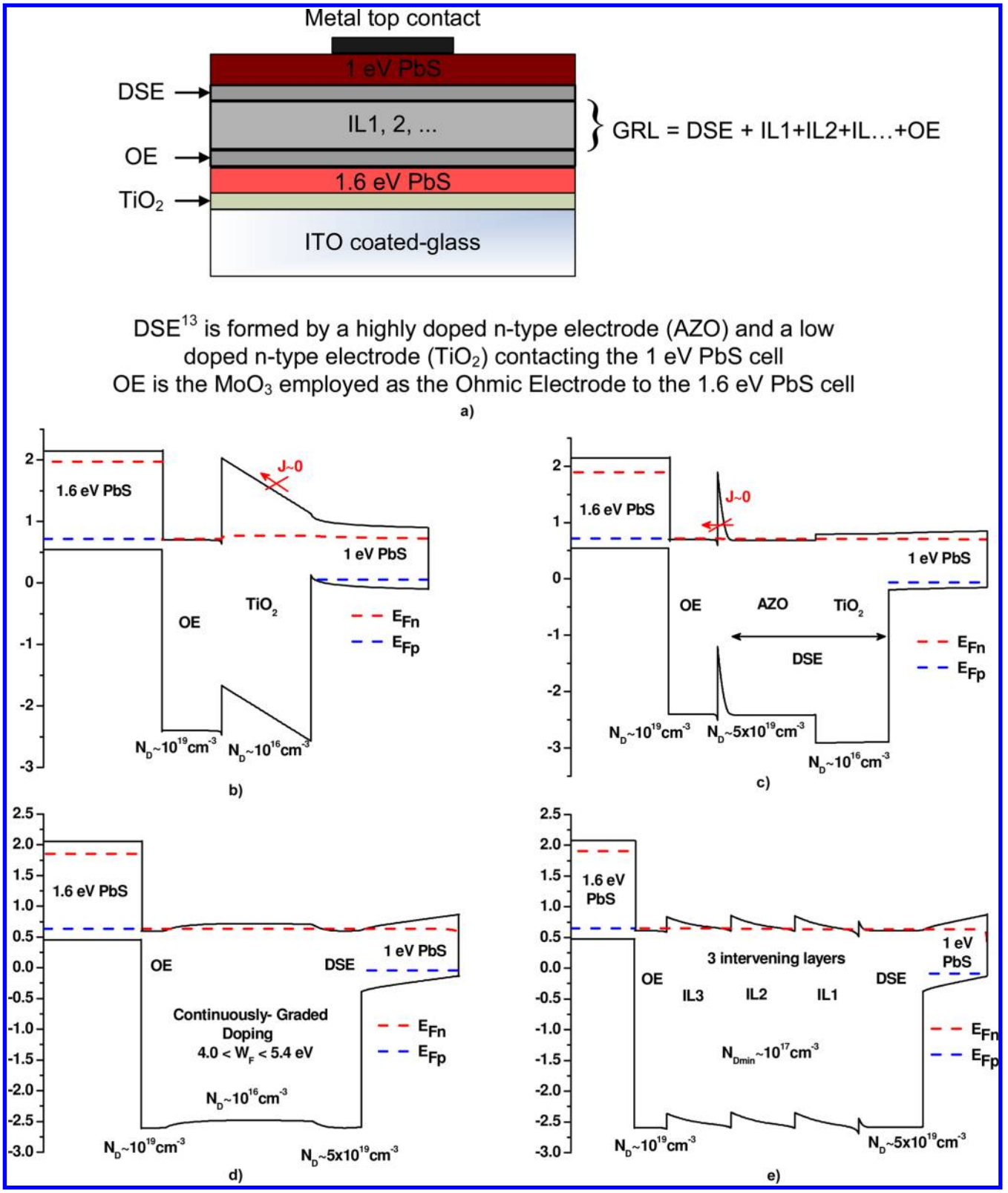

Figure 1. (a) Schematic of a colloidal quantum dot tandem solar cell employing a GRL. The GRL purposes to enable low-impedance connection of the deep work function ohmic electrode (OE) of the front cell with the electron acceptor of the back cell. (b) Equilibrium spatial band diagram for the case of direct contact with the low-doped shallow work function (TiO_2). A thick, higher barrier to electron flow is formed. (c) When a donor supply electrode (DSE) is instead employed, a high tunneling barrier prevents electron flow. (d) An ideal continuously graded recombination layer would eliminate all barriers to electron flow. (e) More realizably, using multiple graded intervening layers of appropriate doping and work functions allows electron transport across the energetic barriers with acceptor resistance for solar applications.

range 4−5 eV, such as TiO_2, ZnO, AZO, ITO, SnO, ZIO, TIO, TZO, and MIO.[3,13−18]

We sought to quantify the requirements for an efficient GRL that connects subcells separated by energy barriers ($\Delta\phi$) in the

dx.doi.org/10.1021/nl300891h | Nano Lett. 2012, 12, 3043−3049

range of 1−1.6 eV. We assumed that the deep work function hole contact (OE) and the shallow work function electron acceptor both had free carrier densities in the 10^{19} cm^{-3} range.[3,13] In our modeling, we accounted for two additive contributors to current density over or through a barrier:

(1) The tunneling current,[19] described via the Fowler−Nordheim equation $J = \lambda ab\phi_b^{-1}F^2 \exp(-\mu b\phi_b^{3/2}/F)$, where $a \sim 1.5 \times 10^{-6}$ A eV V^{-2} and $b \sim 6.8$ $eV^{-3/2}$ V nm^{-1}, $\lambda = 1$, $\mu = (m_e^*/m_e)^{3/2}$, and $eF = \phi_b/x_d$, where ϕ_b is the barrier height and x_d is the barrier width. Tunneling tends to dominate in the case of narrow barriers, a condition facilitated by the use of high doping levels (>10^{18} cm^{-3}). Tunneling will be the dominant mode of transport in designs that employ a small number of highly doped intervening layers separated by high barriers (>0.3 eV).

(2) The thermionic emission current density, described by equation $J = A^{**}T^2\exp(-e\phi_b/kT)(\exp(V/nkT) - 1)$, where A^{**} is the Richardson constant, ϕ_b is the barrier height, and n is the ideality factor of the diode. To pass solar current densities through the thermionic mechanism with acceptably low resistance, the barrier height ϕ_b must typically be less than ∼0.3 eV. Thus a thermionic approach to a graded recombination layer strategy will employ a significant number of low-doped intervening layers, where the total barrier height is divided evenly among the multiple layers.

The details of our modeling assumptions are provided in the Supporting Information (SI1). The materials and spatial band diagrams at open-circuit conditions are shown in Figure 2a,b.

We sought first to determine the design, using a single intermediate work function layer, that would minimize, as much as possible, the doping density required. This would expand the range of practical n-type oxides that could usefully be employed while also minimizing free carrier absorption.

Figure 2c reports the interlayer doping N_{D1} required, as a function of the work functions (W_{F1}) of the intervening layer, to allow a 1 sun ($J \sim 25$ mA/cm^2) to be conveyed with negligible resistive losses. Specifically, to lose less than 0.01 V of operating voltage under solar current densities, $R^*A = V/J <$ ∼1 Ω·cm^2, with R being the resistance and A the device area. We considered the cases of work function differences $\Delta\phi$ of 1, 1.2, and 1.4 eV.

We now discuss the principles for selecting an interlayer work function that minimizes the required interlayer doping. As seen in Figure 2a, electrons flowing from the back to the front cell face two barriers in series, ϕ_{B1} and ϕ_{B2}. Electron transport through ϕ_{B1} is determined by the free carrier density and work function of the shallow work function electron acceptor. It is purely thermionic when ϕ_{B1} is small (<0.25 eV). Thermionic and tunnelling components become comparable to one another for 0.25 < ϕ_{B1} < 0.45 eV. Tunneling dominates in the range 0.45 < ϕ_{B1} < 0.75 eV. For the chosen DSE doping level, solar currents can no longer transit the first barrier when its height exceeds ϕ_{B1} of 0.75 eV.

The preceding limitations ensure that the second barrier ϕ_{B2} will always exceed >0.25 eV. As a result of this fact, combined with the high doping required in the single interlayer case, (>10^{19} cm^{-3} for $\Delta\phi \geq 1$ eV), transport across the second barrier is dominated by tunneling.

We built and characterized (Figure 3) photovoltaic devices employing the single intervening layer GRL design. We used a single ITO intervening layer, thereby implementing the case

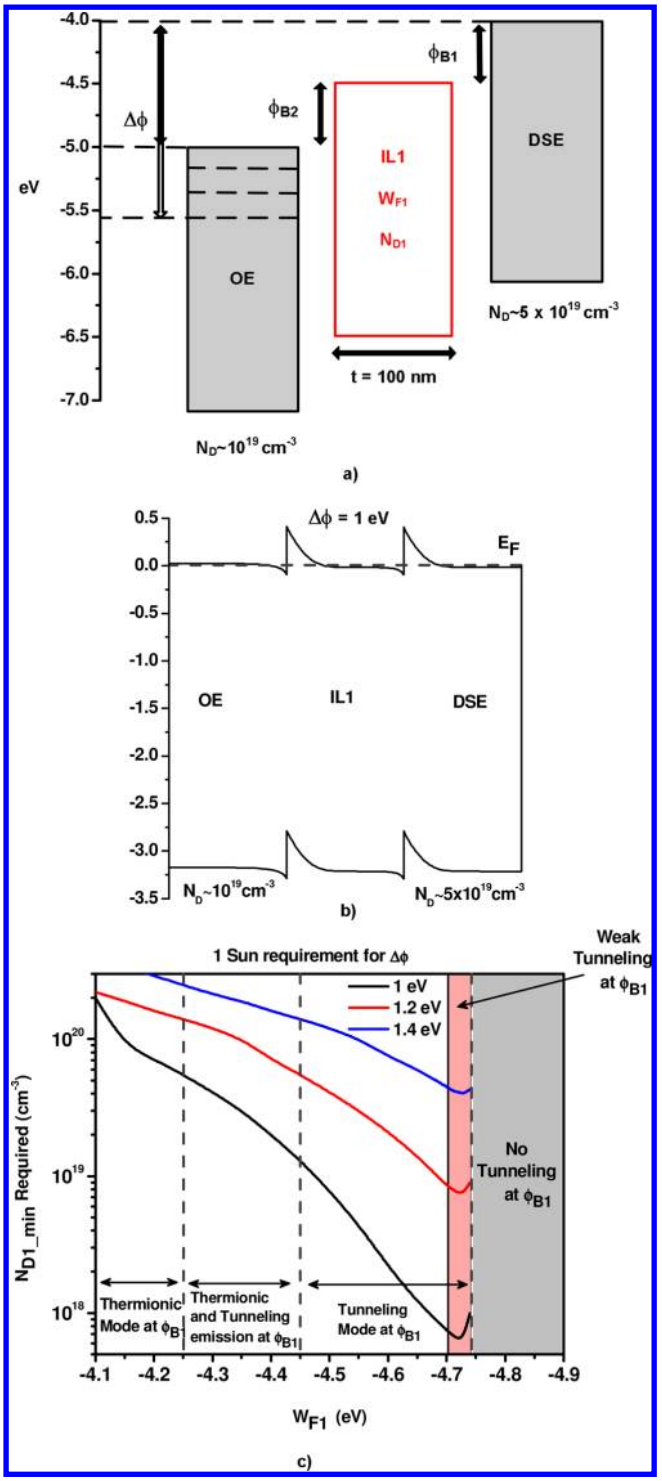

Figure 2. Energy level diagrams of a GRL designed with one intervening layer IL1: (a) before being brought into contact and (b) at equilibrium. (c) The required IL1 doping density (N_{D1}) for a range of work functions W_{F1} to sustain 1 sun with minimal electrical potential loss (0.01 V). The model considered the cases of total work function differences, hence total combined barrier heights $\Delta\phi$, of 1, 1.2, and 1.4 eV. For larger energy separation, one intervening layer is not viable. The different emission modes across ϕ_{B1} are depicted in the figure and explained in the text.

$\Delta\phi \sim 1.3$ eV, ϕ_{B1}∼0.7 eV, and $N_{D1} > 10^{19}$ cm^{-3} (Figure 3a band diagram Supporting Information, SI2). When we replaced the ITO layer with 1 nm metallic Ag nanoclusters, we achieved

dx.doi.org/10.1021/nl300891h | Nano Lett. 2012, 12, 3043−3049

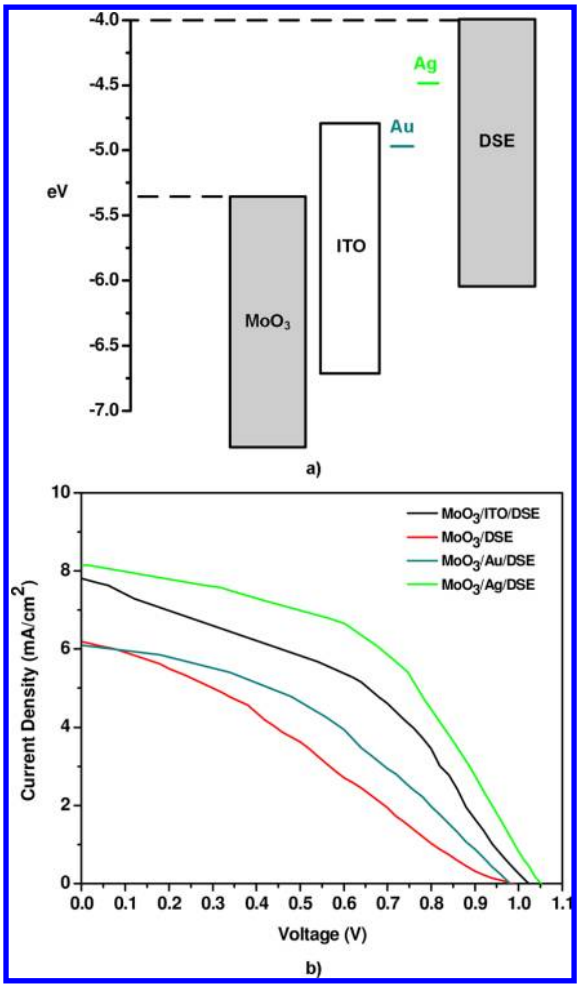

Figure 3. Experimental results. (a) Energy levels of different intervening layers employed in CQD tandem solar cells, and (b) *J*–*V* characteristics of the CQD tandem solar cells without any intervening layers and with ITO, thin Au, and thin Ag as the intervening layer connecting the DSE to MoO_3.

a slightly higher performance with lower series resistance, consistent with the W_{F1} = 4.5 eV case of Figure 2a and the extremely high carrier free carrier density in metallic Ag. Much lower performance results when we employ Au nanoclusters, a fact we attribute to its deeper work function that causes the first barrier to exceed the 0.75 eV threshold for efficient solar operation. We included a control in which we connect the front and back cells directly. A catastrophic loss in performance results: An S-shape curvature is obtained, lowering the open circuit voltage to less than 1 V and the fill factor to less than 30%.

The thin metallic and the ITO interlayers achieve similar performance and are both options of interest. While it achieved the highest performance, the subnanometer thick silver layer has a narrow process window to achieve nanoscale islands. This can result in run-to-run variation, and increasing its thickness to widen this window leads to a failure to fulfill the transparency requirement.[20] Furthermore, metallic layers employed in intermediate layers have been reported to diffuse into the active material of the subcells, leading to loss of high shunt resistance.[21] For these reasons, optimized transparent conductive oxide based interlayer strategies merit further consideration. In addition, in the modeling in Figure 2, we found

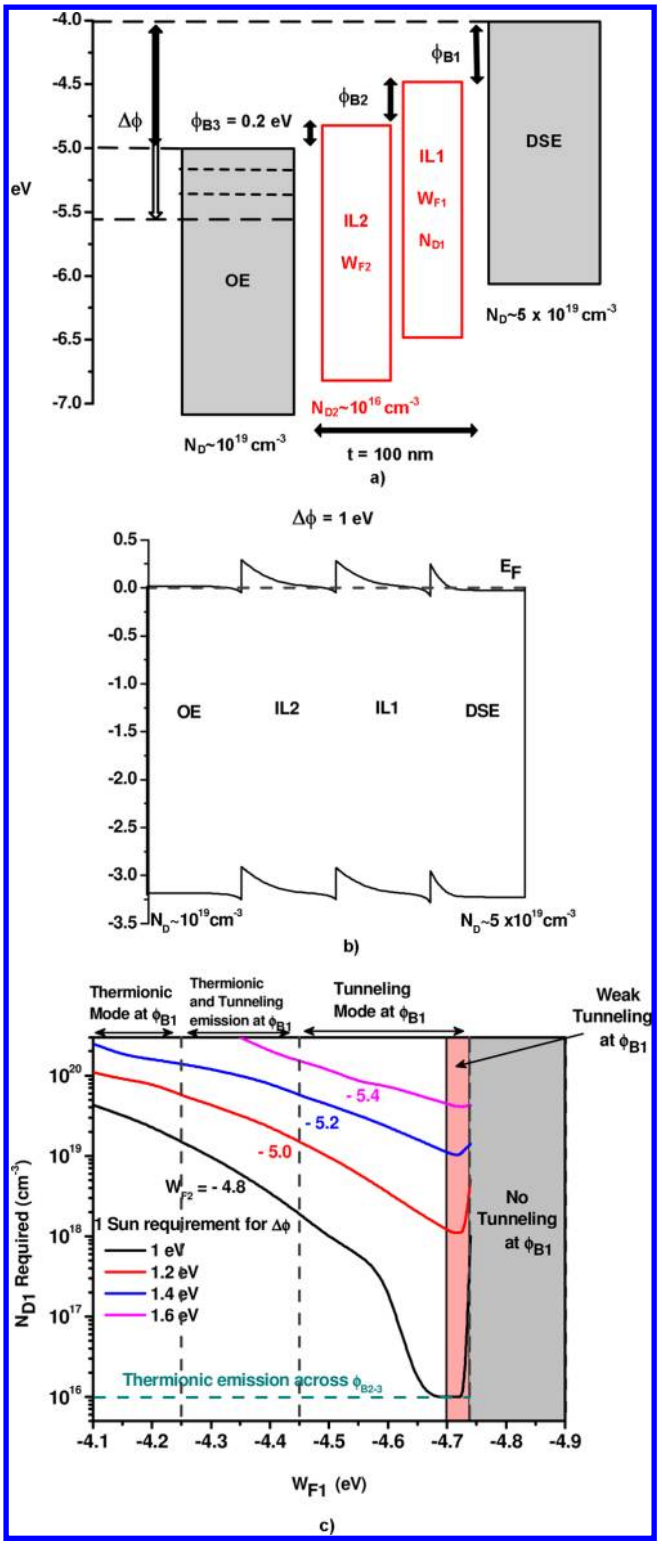

Figure 4. GRL with two intervening layers. Energy level diagrams of a GRL designed with two intervening layers IL1 and IL2 (a) before contact and (b) at equilibrium. With IL2 work function and doping density ($\sim 10^{16}$ cm^{-3}) fixed to ensure thermionic emission across ϕ_{B3}, we plot (c) the required IL1 doping density (N_{D1}) for a range of work functions W_{F1} to sustain 1 sun with minimal electrical potential loss (0.01 V). Modeling was done for a total energy barrier separation $\Delta\phi$ of 1, 1.2, 1.4, and 1.6 eV. For 1 eV $\Delta\phi$, thermionic emission across ϕ_{B2} with minimal N_{D1} required of 10^{16} cm^{-3} occurs for limited values of W_{F1}. Thus, two intervening layers are the maximum number of ILs needed for a 1 eV $\Delta\phi$.

dx.doi.org/10.1021/nl300891h | *Nano Lett.* 2012, 12, 3043–3049

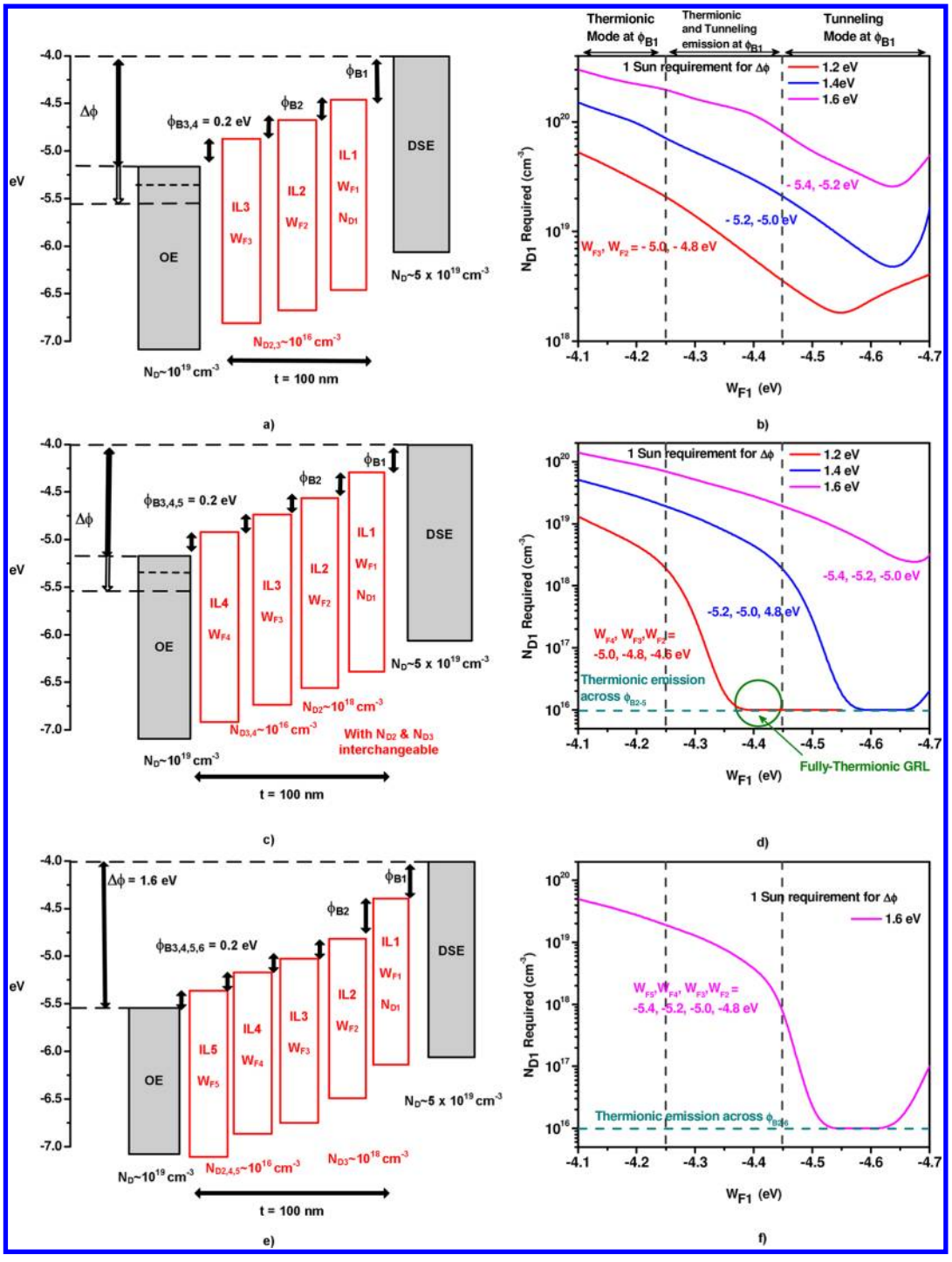

Figure 5. GRL with three, four, and five intervening layers. Energy levels of a GRL designed with (a) three, (c) four, and (e) five intervening layers. We plot the required IL1 doping density (N_{D1}) for a range of work functions W_{F1} to sustain 1 sun with minimal electrical potential loss (0.01 V) with (b) IL2 and IL3 work function and doping density fixed to ensure thermionic emission across $\phi_{B3,4}$, (d) IL2 IL3 and IL4 work function and doping density fixed to ensure thermionic emission across ϕ_{B3-5}, and (f) IL2 IL3 IL4 and IL5 work function and doping density fixed to ensure thermionic emission across ϕ_{B3-6}. Modeling was done for a total energy barrier separation $\Delta\phi$ of 1, 1.2, 1.4, and 1.6 eV. For 1.2 and 1.4 eV $\Delta\phi$, thermionic emission across ϕ_{B2-5} with minimal N_{D1} required occurs for limited values of W_{F1} with four intervening layers. For the latter values of W_{F1} and 1.2 eV $\Delta\phi$, emission across ϕ_{B1} is also thermionic making the total electron flow from the DSE to the OE purely thermionic. Four intervening layers are the maximum number of ILs needed for a 1.2 and 1.4 eV $\Delta\phi$, while 5 intervening layers are needed to reach the minimal doping $N_{D1} \sim 10^{16}$ cm^{-3} for 1.6 eV $\Delta\phi$.

that work function differences greater than 1.4 eV can not successfully be spanned using a single intervening layer.

We therefore explored multiple interlayer strategies that would reduce significantly the doping requirement on the intervening layers and expand the range of work function differences that can be connected. We were particularly interested in lowering the required doping down to the ~10^{16} cm^{-3}, that is easily attained using available low-temperature deposited n-type oxides.[3,13−18]

When a pair of interlayers is employed (Figure 4) and when the second interlayer uses a modest doping of ~10^{16} cm^{-3} and

dx.doi.org/10.1021/nl300891h | Nano Lett. 2012, 12, 3043−3049

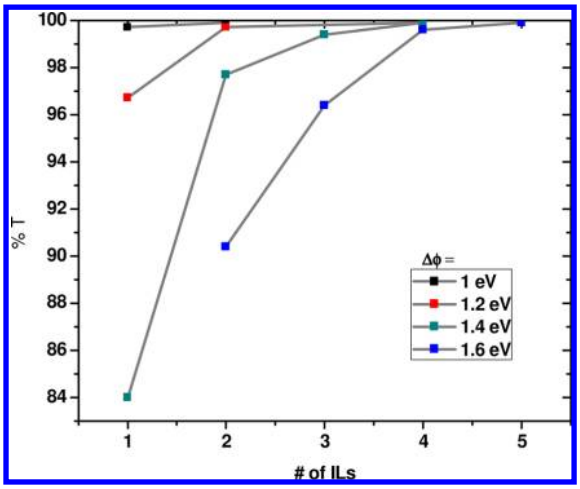

Figure 6. Optical transmission, parametrized as a function of the number of intervening layers employed, for the different GRL designs summarized in Table 1.

Table 1. Summary of the Design Rules of GRLs Sustaining Solar Intensities at Minimal Photovoltage Loss

Δϕ (eV)	N_D required (cm^{-3}) of IL1	IL2	IL3	IL4	IL5	$t_{per\ layer}$ [$] (nm)
1	6.3×10^{17} *	…	…	…	…	100
	10^{16}	10^{16}	…	…	…	50
1.2	7.5×10^{18} *	…	…	…	…	100
	1.2×10^{18} *	10^{16}	…	…	…	50
	2.4×10^{18}	10^{16}	10^{16}	…	…	33
	10^{16}	$10^{18} \longleftrightarrow 10^{16}$		10^{16}	…	25
1.4	4×10^{19} *	…	…	…	…	100
	1×10^{19} *	10^{16}	…	…	…	50
	4×10^{18} *	10^{16}	10^{16}	…	…	33
	10^{16}	$10^{18} \longleftrightarrow 10^{16}$		10^{16}	…	25
1.6	…	…	…	…	…	…
	4.5×10^{19} *	10^{16}	…	…	…	50
	2.5×10^{19} *	10^{16}	10^{16}	…	…	33
	2.5×10^{18} *	$10^{18} \longleftrightarrow 10^{16}$		10^{16}	…	25
	10^{16}	10^{18}	10^{16}	10^{16}	10^{16}	20

[$]Thickness per layer. *Tunneling mode through ϕ_{B2}

a low barrier height ϕ_{B3} of 0.2 eV, efficient and purely thermionic emission is achieved across ϕ_{B3}. Now, for a work function difference $\Delta\phi$ of 1 eV between the cells, two intervening layers of doping density $\sim 10^{16}$ cm^{-3} are sufficient to sustain solar current densities.

We proceeded to ascertain the number of interlayers required to enable solar currents to transit larger 1.2, 1.4, and 1.6 eV interjunction barriers using modestly doped interlayers. For $\Delta\phi$ of 1.2 and 1.4 eV, four intervening layers are sufficient, while five are necessary for a 1.6 eV energy separation (Figure 5c–f). For the 1.2 eV $\Delta\phi$ case, four intervening layers (Figure 5d) allow for purely thermionic emission across the entire GRL including ϕ_{B1}, which for smaller numbers of interlayers is tunnelling dominated.

It was assumed until this point that the back cell is contacted using a highly doped shallow work function contact. The use of multiple interlayers can also relax this requirement. Adding one extra interlayer can ensure that thermionic emission occurs across all barriers including ϕ_{B1} and obviate the need for the heavily doped donor supply electrode (DSE).[13]

We now evaluate the benefits, in terms of optical transmission in the infrared spectral region, that are accrued when low-doped intervening layers (with reduced free carrier absorption) are employed (Supporting Information, SI3). As seen in Table 1, considering the case of $\Delta\phi$ larger than 1.2 eV, the use of 1 or 2 intervening layers demands a high doping ($>10^{19}$ cm^{-3}), which leads to high optical loss. Replacing the highly doped layers with multiple low-doped layers (Figure 6) reduces optical loss appreciably. Only by using a GRL consisting of at least 3 intervening layers can optical loss through the GRL be kept below 5% for large work function differences $\Delta\phi$ of 1.6 eV or greater.

We summarize the design of an efficient GRL of interest in a variety of solution-processed solar cells, including colloidal quantum dot and organic photovoltaics. To achieve a high transmittance and a wide process window, intervening layers based on low-doped oxides, with their low free carrier absorption, are desired. A work function difference of 1 eV can be spanned in a number of ways. A single optimal work function interlayer is sufficient but relies on a relatively high doping of 1×10^{19} cm^{-3}. A pair of interlayers having a much lower 1×10^{16} cm^{-3} can efficiently span this work function difference. Adding a further interlayer can obviate the need for the highly doped donor supply electrode. Higher numbers of interlayers allow successful spanning of larger work function differences along the same principles. Selection of work functions of these interlayers according to the prescriptions of this work is readily implemented using the wide range of room temperature deposited conductive oxides in the literature.[13−18,20−25]

■ ASSOCIATED CONTENT

Ⓢ Supporting Information

Methods, equations, and modeling details. This material is available free of charge via the Internet at http://pubs.acs.org.

■ AUTHOR INFORMATION

Corresponding Author

*E-mail: ted.sargent@utoronto.ca

Author Contributions

[†]These authors contributed equally

Notes

The authors declare no competing financial interest.

■ ACKNOWLEDGMENTS

This publication is based in part on work supported by an award (no. KUS-11-009-21) made by King Abdullah University of Science and Technology (KAUST), by the Ontario Research Fund Research Excellence Program, by the Natural Sciences and Engineering Research Council (NSERC) of Canada, and by Angstrom Engineering and Innovative Technology. The authors would also like to acknowledge the assistance of Larissa Levina, Armin Fisher, Elenita Palmiano, Remigiusz Wolowiec, and Damir Kopilovic. G.I.K. acknowledges NSERC support in the form of Alexander Graham Bell Canada Graduate Scholarship. X.W. was partially supported by an Ontario Post Doctoral Fellowship from the Ontario Ministry of Research and Innovation.

■ REFERENCES

(1) Sargent, E. H. *Nat Photon* **2009**, *3*, 325−331.
(2) Henry, C. H. *J. Appl. Phys.* **1980**, *51*, 4494−4500.

(3) Wang, X.; Koleilat, G. I.; Tang, J.; Liu, H.; Kramer, I. J.; Debnath, R.; Brzozowski, L.; Barkhouse, D. A. R.; Levina, L.; Hoogland, S.; Sargent, E. H. *Nat Photon* **2011**, *5*, 480−484.
(4) Dou, L.; You, J.; Yang, J.; Chen, C.-C.; He, Y.; Murase, S.; Moriarty, T.; Emery, K.; Li, G.; Yang, Y. *Nat Photon* **2012**.
(5) Lamorte, M. F.; Abbott, D. H. *Sol. Cells* **1983**, *9*, 311−326.
(6) Yamaguchi, M.; Takamoto, T.; Araki, K.; Ekins-Daukes, N. *Sol. Energy* **2005**, *79*, 78−85.
(7) King, R. R.; et al. *Appl. Phys. Lett.* **2007**, *90*, 183516.
(8) Hiramoto, M.; Suezaki, M.; Yokoyama, M. *Chem. Lett.* **1990**, *19*, 327−330.
(9) Yakimov, A.; Forrest, S. R. *Appl. Phys. Lett.* **2002**, *80*, 1667−1669.
(10) Gao, J.; Perkins, C. L.; Luther, J. M.; Hanna, M. C.; Chen, H.-Y.; Semonin, O. E.; Nozik, A. J.; Ellingson, R. J.; Beard, M. C. *Nano Lett.* **2011**, *11*, 3263−3266.
(11) Brown, P. R.; Lunt, R. R.; Zhao, N.; Osedach, T. P.; Wanger, D. D.; Chang, L.-Y.; Bawendi, M. G.; Bulović,, V. *Nano Lett.* **2011**, *11*, 2955−2961.
(12) Wang, X.; Koleilat, G. I.; Fischer, A.; Tang, J.; Debnath, R.; Levina, L.; Sargent, E. H. *ACS Appl. Mater. Interfaces* **2011**, *3*, 3792−3795.
(13) Koleilat, G. I.; Wang, X.; Labelle, A. J.; Ip, A. H.; Carey, G. H.; Fischer, A.; Levina, L.; Brzozowski, L.; Sargent, E. H. *Nano Lett.* **2011**, *11*, 5173−5178.
(14) Singh, A. V.; Mehra, R. M.; Buthrath, N.; Wakahara, A.; Yoshida, A.. *J. Appl. Phys.* **2001**, *90* (11), 5661−5665.
(15) Ellmer, K.; Vollweiler, G *Thin Film Solids* **2006**, *496* (1), 104−111.
(16) Ghosh, S.; Hoogland, S.; Sukhovatkin, V.; Levina, L.; Sargent, E. H. *Appl. Phys. Lett.* **2011**, *99*, 101102.
(17) Kuo, F.-L.; Li, Y.; Solomon, M.; Du, J.; Shepherd, N. D. *J. Phys. D: Appl. Phys.* **2012**, *45*, 065301.
(18) Minami, T.; Miyata, T.; Yamamoto, T. *Surf. Coat. Technol.* **1998**, *108−109*, 583−587.
(19) Forbes, R. G. J. *Vac. Sci. Technol., B* **2008**, *26*, 788−793.
(20) Bulíř, J.; Novotný, M.; Lynnykova, A.; Lančok, J. *J. Nanophotonics* **2011**, *5*, 051511−051511−10.
(21) Xue, J. G.; Uchida, S.; Rand, B. P.; Forrest, S. R. *Appl. Phys. Lett.* **2004**, *85*, 5757−5759.
(22) Kim, J. Y.; Lee, K.; Coates, N. E.; Moses, D.; Nguyen, T.-Q.; Dante, M.; Heeger, A. J. *Science* **2007**, *317*, 222−225.
(23) Jiang, X.; Wong, F. L.; Fung, M. K.; Lee, S. T. *Appl. Phys. Lett.* **2003**, *83*, 1875−1877.
(24) Hyun, B.-R.; Zhong, Y.-W.; Bartnik, A. C.; Sun, L.; Abruña, H. D.; Wise, F. W.; Goodreau, J. D.; Matthews, J. R.; Leslie, T. M.; Borrelli, N. F. *ACS Nano* **2008**, *2*, 2206−2212.
(25) Meyer, J.; Shu, A.; Kröger, M.; Kahn, A. *Appl. Phys. Lett.* **2010**, *96*, 133308.